

A Deep Variational Bayesian Framework for Blind Image Deblurring

Hui Wang, Zongsheng Yue, Qian Zhao*, Deyu Meng

School of Mathematics and Statistics, Xi'an Jiaotong University
huiwang2019@stu.xjtu.edu.cn, zsyzam@gmail.com,
{timmy.zhaoqian, dymeng}@xjtu.edu.cn

Abstract

Blind image deblurring is an important yet very challenging problem in low-level vision. Traditional optimization based methods generally formulate this task as a maximum-a-posteriori estimation or variational inference problem, whose performance highly relies on the handcraft priors for both the latent image and the blur kernel. In contrast, recent deep learning methods generally learn, from a large collection of training images, deep neural networks (DNNs) directly mapping the blurry image to the clean one or to the blur kernel, paying less attention to the physical degradation process of the blurry image. In this paper, we present a deep variational Bayesian framework for blind image deblurring. Under this framework, the posterior of the latent clean image and blur kernel can be jointly estimated in an amortized inference fashion with DNNs, and the involved inference DNNs can be trained by fully considering the physical blur model, together with the supervision of data driven priors for the clean image and blur kernel, which is naturally led to by the evidence lower bound objective. Comprehensive experiments are conducted to substantiate the effectiveness of the proposed framework. The results show that it can not only achieve a promising performance with relatively simple networks, but also enhance the performance of existing DNNs for deblurring.

1 Introduction

Image deblurring is an important problem in the field of image restoration and has attracted wide attention with a long history [39, 8, 5]. The goal of deblurring is to recover the underlying clean image from an observed blurry one. Such a blurry image can be resulted by different reasons, such as defocusing and camera shaking, which can in general be modeled as (assuming the blur process is uniform and spatially invariant)

$$\mathbf{y} = \mathbf{h} * \mathbf{z} + \mathbf{n}, \quad (1)$$

where \mathbf{y} is the blurry image, \mathbf{z} is the corresponding clean one, \mathbf{h} is the blur kernel (point spread function), \mathbf{n} is the noise, often modeled as additive white Gaussian noise, and $*$ denotes the 2D convolution operator. When the blur kernel \mathbf{h} is unknown, we need to simultaneously estimate \mathbf{h} and \mathbf{z} solely from the given observation \mathbf{y} , which is commonly referred as blind image deblurring or blind deconvolution. It is a highly ill-posed inverse problem, since there can be different pairs of \mathbf{z} and \mathbf{h} explaining one same blurred image \mathbf{y} .

Many different methods have been proposed to address this problem, which can be mainly categorized into two groups, i.e., optimization-based methods and deep learning ones. Traditional optimization-based methods, from the probabilistic perspective, generally formulate the image deblurring task as a maximum-a-posteriori (MAP) estimation problem [23, 43, 49, 34, 35, 27, 22] or Bayesian

*Corresponding author.

posterior inference (specifically variational inference (VI)) one [8, 56, 2], by properly designing priors to both the to-be-estimated image [49, 34, 35, 22, 8, 27] and blur kernel [28, 56]. However, the manually designed priors are still subjective and may not precisely characterize the intrinsic distributions of natural images and blur kernels in real world, limiting the performance of a deblurring algorithm. Besides, solving the complex optimization usually causes heavy computational cost, which is always unaffordable in real applications. Recently, motivated by their great success in computer vision, especially for other image restoration problems, [6, 54], deep learning methods have also attracted increasing attention in image deblurring research. Early attempts along this line used deep neural networks (DNNs) as a component of traditional methods, e.g., estimating the blur kernel [45, 11, 42, 4]. Later, learning an explicit mapping from a blurred image to its deblurred one in an end-to-end fashion has become a dominant methodology [17, 30, 46]. This approach is especially superior in extracting underlying knowledge from large datasets and fast deblurring for test images.

Existing deep deblurring methods mainly focus on designing fancy network architectures, while pay less attention to make full use of the information delivered by physical blur model (1), which limits further performance improvement for them. In contrast, (1) plays a crucial role for achieving a promising performance in optimization based methods, especially Bayesian ones [8, 26, 32]. Based on these observations, and also inspired by recent advances in deep Bayesian modeling for image restoration [50], we propose a deep variational Bayesian framework for training deblurring neural networks in the blind setting, aiming at simultaneously estimating the clean image and blur kernel. Specifically, under the generative model of blurry image, we construct the variational distributions parameterized by DNNs to approximate the true posteriors of both the latent clean image and blur kernel, and learn the network parameters by optimizing the evidence lower bound (ELBO). After training, the inference networks can then be directly used to approximate the corresponding posteriors of clean image and blur kernel in an amortized way, efficiently from an observed blurry image.

The main advantages of the proposed method can be summarized as follows. First, by virtue of the Bayesian generative model, the physical blur model (1) can be naturally encoded as the likelihood term in the ELBO to guide learning the inference networks. Therefore, the inference networks for the clean image and blur kernel can both be jointly trained under the supervision of data driven priors, and interact with each other due to the likelihood. Second, the proposed framework provides, in principle, a natural unification of previous methodologies that consider kernel information for training deblurring DNNs, in a concise Bayesian way, and thus is expected to achieve a better performance. Third, our framework can also be straightforwardly incorporated with any existing end-to-end DNNs to enhance their performance. All of these advantages have been substantiated by our experiments.

The remainder of this paper is organized as follows: Section 2 introduces the related studies. Section 3 presents the proposed deep Bayesian framework, including Bayesian generative model, deep VI procedure and network architectures. Section 4 shows the experimental results and analyses. Final conclusion is made in Section 5.

2 Related Work

Optimization based methods The main focus along this research line is to design priors that can precisely characterize the intrinsic structures of clean images and blur kernels, in order to make the ill-posed blind deblurring problem solvable. A series of priors have been developed for clean images, including total variation [5], sparsity of gradients [8, 43], hyper-Laplacian [22], L_0 -norm prior [49, 34], internal patch prior [27] and dark channel prior [35]. For blur kernels, the aforementioned priors can still be applied, while there are also some specifically designed priors, e.g., Dirichlet prior [28, 56] and piecewise-linear prior [31]. After specifying the priors, such a blind image deblurring problem can be formulated as a MAP estimation [43, 49, 34, 35, 27, 22] or Bayesian posterior inference (more specifically VI) [8, 56] problem, and solved by off-the-shelf optimization tools.

Deep learning based methods Having witnessed the great success in other fields, deep learning has also been investigated in dealing with the image deblurring task. Early methods treat DNNs as a part of traditional optimization based ones, by virtue of their prediction ability. For example, Schuler *et al.* [42] designed a convolutional neural network (CNN) to simulate iterative optimization for image deblurring. Sun *et al.* [45] used a CNN to classify the blur kernel in patch-level. Gong *et al.* [11] went further to predict the motion flow in a pixel-level. Chakrabarti [4] used CNN to predict the kernel in the frequency domain. It is then gradually popular to directly parameterize the mapping from a blurry

image and its clean one with CNNs in a kernel free paradigm, and then learn the parameters by a large collection of blurry-clean image pairs. Hradiš *et al.* [17] directly predicted latent clean images from observed blurred images by a fully CNN. Nah *et al.* [30] introduced a multi-scale CNN to directly recover the latent clean image. Tao *et al.* [46] improved the architecture by using a scale-recurrent network and a ConvLSTM [44] layer. The generative adversarial network (GAN) [12] is also applied to image deblurring, e.g., Kupyn *et al.* [24] utilized the Wasserstein GAN [1] to learn a generator that restores the latent image. Recently, there are some studies that borrow fundamental principles from traditional methods. Pan *et al.* [32] introduce the consistency loss motivated from the likelihood in traditional methods. Cai *et al.* [3] embed the dark and bright channel prior to a deep multi-scale neural network. Ren *et al.* [37] tried to directly solve the traditional blind deblurring optimization, while constrain the solution space by deep image priors [47].

3 Deep Variational Bayesian Framework for Blind Image Deblurring

Let $\mathcal{D} = \{\mathbf{x}^{(j)}, \mathbf{y}^{(j)}, \mathbf{k}^{(j)}\}_{j=1}^N$ be the training dataset, where $\mathbf{x}^{(j)}$, $\mathbf{y}^{(j)}$ and $\mathbf{k}^{(j)}$ denote the clean image, blurry image and blur kernel, respectively, in the j th training tuple, and N be the number of training tuples. Our goal is to construct parametric forms with DNNs to approximate the posteriors of both clean image and blur kernel, given only the observed blurry image, under the Bayesian framework. With these parametric variational posteriors trained on \mathcal{D} , we can directly infer the posterior distributions of both clean image and blur kernel from a test blurry image. Note that in practical training deblurring datasets [30], for a blurry image, the corresponding “clean” image is often obtained by complicated acquisition process, which might not be the exact latent clean image. Besides, the groundtruth blur kernels are also unavailable. Nevertheless, these two issues can be naturally addressed within our Bayesian formulation.

3.1 Bayesian Model of Blind Image Deblurring with Data Driven Priors

Let $(\mathbf{x}, \mathbf{y}, \mathbf{k})$, with $\mathbf{x} \in \mathbb{R}^{h \times w}$, $\mathbf{y} \in \mathbb{R}^{h \times w}$, and $\mathbf{k} \in \mathbb{R}^{h' \times w'}$, be any training tuple in \mathcal{D} , where $h \times w$ and $h' \times w'$ are respectively the sizes of image and kernel. As aforementioned, the “clean” image \mathbf{x} and blur kernel \mathbf{k} might be inaccurate or unavailable, and thus we introduce notations \mathbf{z} and \mathbf{h} for the latent clean image and blur kernel, respectively. With these notations, we can build our Bayesian model for blind image deblurring as follows.

Likelihood: Considering the physical blur model (1), we can have the following likelihood for the observed blurry image \mathbf{y} , given the latent clean image \mathbf{z} and blur kernel \mathbf{h} [8, 29]:

$$p(\mathbf{y}|\mathbf{z}, \mathbf{h}) = \prod_{i=1}^d \mathcal{N}(y_i; (\mathbf{h} * \mathbf{z})_i, \sigma^2), \quad (2)$$

where $\mathcal{N}(\cdot; \mu, \sigma^2)$ denotes the Gaussian distribution with mean μ and variance σ^2 , subscript i denotes the i th pixel within the image (by taking the image matrix as a vector) and $d = hw$ for notation convenience. It should be mentioned that, in this work, we treat the variance σ^2 as a hyper-parameter to reduce the complexity of overall model. Nevertheless, we can also treat it as a to-be-estimated variable and learn its posterior distribution from data as in [50].

To complete the full Bayesian model, we then need introduce priors to \mathbf{z} and \mathbf{h} . Different from that in traditional optimization based methods, where the priors were specified in a subjective way, we place these priors in a data driven fashion with the aid of training set \mathcal{D} , which is detailed in the following.

Data Driven Prior for Clean Image: As mentioned before, \mathbf{x} in the training set might not exactly be the latent clean image \mathbf{z} . Nevertheless, it can be expected that \mathbf{x} is close to \mathbf{z} , and thus provide strong prior information to it. Thus, we can naturally assume the prior distribution of \mathbf{z} as

$$p(\mathbf{z}) = \prod_{i=1}^d \mathcal{N}(z_i; x_i, \varepsilon_0^2) \quad (3)$$

where ε_0^2 is a hyper-parameter, which measures the uncertainty of \mathbf{z} . Since typical deblurring datasets are carefully collected, it is expected that \mathbf{x} is close enough to \mathbf{z} , and we can correspondingly assume a small ε_0^2 . In the extreme case that ε_0^2 tends to 0, the prior degenerates to the Dirac distribution with all mass centered at \mathbf{x} . We will empirically analyze the effect of ε_0^2 in our experiments.

Data Driven Prior for Blur Kernel: Specifying a proper prior distribution for the blur kernel is more difficult, since there is a constraint that the sum of all elements in a blur kernel should equal to

1. Fortunately, Dirichlet distribution defined on a simplex well meet this requirement. Its probability density function, with parameter $\alpha = (\alpha_1, \dots, \alpha_M)$, $\alpha_m > 0$, $m = 1, \dots, M$ has the following form:

$$\text{Dir}(\pi; \alpha) = \frac{1}{Z(\alpha)} \prod_{m=1}^M \pi_m^{\alpha_m-1}, \quad 0 < \pi_m < 1, \quad m = 1, \dots, M, \quad (4)$$

where $Z(\alpha) = \prod_{m=1}^M \Gamma(\alpha_m) / \Gamma(\sum_{m=1}^M \alpha_m)$ is the normalizing factor, with $\Gamma(\cdot)$ being the gamma function. Besides, the mean and variance are given by, denoting $\alpha_0 = \sum_{m=1}^M \alpha_m$,

$$\mathbb{E}[\pi_m] = \alpha_m / \alpha_0, \quad \text{Var}[\pi_m] = (\alpha_m(\alpha_0 - \alpha_m)) / (\alpha_0^2(\alpha_0 + 1)). \quad (5)$$

With the above knowledge, we can naturally place a Dirichlet prior to the latent blur kernel \mathbf{h} , and the problem is how to set its hyper-parameter. Since \mathbf{k} , if available, in the training set should provide strong information to \mathbf{h} , it is reasonable to assume $\mathbb{E}[\mathbf{h}] = \mathbf{k}$. Also, as can be seen from (5), the mean of a Dirichlet distribution remains the same under a scaling transformation of parameters. Therefore, we can introduce the following prior distribution to \mathbf{h} :

$$p(\mathbf{h}) = \text{Dir}(\mathbf{h}; c\mathbf{k}) \propto \prod_{i'=1}^{d'} h_{i'}^{ck_{i'}-1}, \quad (6)$$

where $d' = h'w'$ for convenience, and $c > 0$ is a scaling factor to be tuned. Although hyper-parameter c does not affect the mean provided \mathbf{k} being specified, it does determine the variance according to (5), and correspondingly the prior uncertainty of \mathbf{h} . Thus, if \mathbf{k} is given in the training set, we may set c to a relatively larger value, which results in a smaller prior uncertainty for \mathbf{h} . In contrast, if \mathbf{k} is unavailable, we can only roughly estimate it from the given \mathbf{y} and \mathbf{x} , and it is better to set c small to avoid the inaccurate prior information being too strong.

Posterior Inference Goal: Giving both the likelihood and priors, the goal then turns to inferring the posterior distribution of the latent variables \mathbf{z} and \mathbf{h} from the observed blurry image \mathbf{y} , which, by the Bayes' rule, can be theoretically formulated as

$$p(\mathbf{z}, \mathbf{h} | \mathbf{y}) \propto p(\mathbf{z}, \mathbf{h}, \mathbf{y}) = p(\mathbf{y} | \mathbf{z}, \mathbf{h}) p(\mathbf{z}) p(\mathbf{h}). \quad (7)$$

Exactly computing this posterior is intractable, especially for a test image out of the training set. Therefore, we turn to constructing the approximate posterior in an amortized way [21, 38] with DNNs, and then train the inference networks on the training set. After that, the trained networks can be used to directly infer the posterior of \mathbf{z} and \mathbf{h} by input a test blurry image \mathbf{y} .

3.2 Variational Formulations of Posterior

In order to achieve the goal mentioned in the previous subsection, we first need to construct the variational form of the posterior, denoted as $q(\mathbf{z}, \mathbf{h} | \mathbf{y})$, to approximate the intractable true posterior in (7). Since $p(\mathbf{z}, \mathbf{h} | \mathbf{y})$ is a joint distribution of \mathbf{z} and \mathbf{h} , there are multiple ways to formulate the variational posterior, and we discuss two possible ones according to the way of inferring \mathbf{z} .

Kernel-free Inference Structure for \mathbf{z} : The basic mean-field assumption for $q(\mathbf{z}, \mathbf{h} | \mathbf{y})$ is

$$q(\mathbf{z}, \mathbf{h} | \mathbf{y}) = q(\mathbf{z} | \mathbf{y}) q(\mathbf{h} | \mathbf{y}), \quad (8)$$

which assumes the conditional independence between \mathbf{z} and \mathbf{h} given \mathbf{y} . Then we further specify $q(\mathbf{z} | \mathbf{y})$ and $q(\mathbf{h} | \mathbf{y})$ with the same families as $q(\mathbf{z})$ and $q(\mathbf{h})$, respectively:

$$q_{\Psi}(\mathbf{z} | \mathbf{y}) = \prod_{i=1}^d \mathcal{N}(z_i; \mu_i(\mathbf{y}; \Psi), m_i^2(\mathbf{y}; \Psi)), \quad q_{\Phi}(\mathbf{h} | \mathbf{y}) = \text{Dir}(\mathbf{h}; \xi(\mathbf{y}; \Phi)), \quad (9)$$

where Ψ denotes the parameters of the inference network for \mathbf{z} , which takes \mathbf{y} as its input and outputs the mean $\mu_i(\mathbf{y}; \Psi)$ and variance $m_i^2(\mathbf{y}; \Psi)$, and thus can be recognized as *Deblur-Net*; similarly, Φ parameterizes the inference network for \mathbf{h} , which also takes \mathbf{y} as input while outputs the parameters $\xi(\mathbf{y}; \Phi) = (\xi_1(\mathbf{y}; \Phi), \dots, \xi_{d'}(\mathbf{y}; \Phi))$, and thus can be referred to as *Kernel-Net*.

Kernel-dependent Inference Structure for \mathbf{z} : Another formulation for variational posterior $q(\mathbf{z}, \mathbf{h} | \mathbf{y})$ is obtained by conditional probability rule:

$$q(\mathbf{z}, \mathbf{h} | \mathbf{y}) = q(\mathbf{z} | \mathbf{h}, \mathbf{y}) q(\mathbf{h} | \mathbf{y}), \quad (10)$$

where the posterior of z is also conditioned on h in addition to y . This dependence can be easily achieved by taking both h and y as the inputs of *Deblur-Net*, leading to following variational form:

$$q_{\Psi}(z|h, y) = \prod_{i=1}^d \mathcal{N}(z_i; \mu_i(h, y; \Psi), m_i^2(h, y; \Psi)). \quad (11)$$

This parameterization is rational, since the blur kernel, if accurately estimated, can provide useful information for deblurring an image. The variational form of $q_{\Phi}(h|y)$ remains the same as in (9).

Remark: Mathematically, it is also hold that $q(z, h|y) = q(h|z, y)q(z|y)$, which leads to another valid variational posterior formulation. However, considering that our ultimate goal is to deblur y , this formulation is less attractive, since it requires estimating z first before inferring h .

3.3 Network Learning with Evidence Lower Bound

After the variational posterior parameterized by DNNs having be constructed, we need to derive the evidence lower bound (ELBO), which acts as the objective function for learning the network parameters Ψ and Φ . For notation convenience, we simplify $\mu_i(y; \Psi)$ and $\mu_i(h, y; \Psi)$ to $\mu_i, m_i^2(y; \Psi)$ and $m_i^2(h, y; \Psi)$ to m_i^2 , and $\xi_{i'}(y; \Phi)$ to $\xi_{i'}$ in the following.

Based on conventional decomposition of marginal likelihood in VI, we can get

$$\log p(y) = \mathcal{L}(y; \Psi, \Phi) + D_{KL}(q(z, h|y)||p(z, h|y)), \quad (12)$$

where $D_{KL}(\cdot||\cdot)$ is the KL divergence between two distributions, and $\mathcal{L}(y; \Psi, \Phi)$ is the ELBO we want to maximize. According to the two variational formulations (8) and (10), we correspondingly have the following two ELBOs (derivations are provided in Appendix A):

$$\mathcal{L}_{KF}(y; \Psi, \Phi) = \mathbb{E}_{q(z|y)q(h|y)}[\log p(y|h, z)] - D_{KL}(q(z|y)||p(z)) - D_{KL}(q(h|y)||p(h)), \quad (13)$$

and

$$\mathcal{L}_{KD}(y; \Psi, \Phi) = \mathbb{E}_{q(z|h, y)q(h|y)}[\log p(y|h, z)] - \mathbb{E}_{q(h|y)}[D_{KL}(q(z|h, y)||p(z))] - D_{KL}(q(h|y)||p(h)), \quad (14)$$

where we omit the subscripts in $q_{\Psi}(z|h, y)$, $q_{\Psi}(z|h, y)$ and $q_{\Phi}(h|y)$. The KL divergence terms in the above two equations can then be calculated analytically as follows:

$$D_{KL}(q(z|y)||p(z)) = D_{KL}(q(z|h, y)||p(z)) = \sum_{i=1}^d \left\{ \frac{(\mu_i - x_i)^2}{2\varepsilon_0^2} + \frac{1}{2} \left[\frac{m_i^2}{\varepsilon_0^2} - \log \frac{m_i^2}{\varepsilon_0^2} - 1 \right] \right\}, \quad (15)$$

$$\begin{aligned} D_{KL}(q(h|y)||p(h)) &= \log \Gamma\left(\sum_{i'=1}^{d'} \xi_{i'}\right) - \log \Gamma\left(\sum_{i'=1}^{d'} ck_{i'}\right) - \sum_{i'=1}^{d'} \log \Gamma(\xi_k) \\ &\quad + \sum_{i'=1}^{d'} \log \Gamma(ck_{i'}) + \sum_{i'=1}^{d'} (\xi_{i'} - ck_{i'}) \left(\psi_0(\xi_{i'}) - \psi_0\left(\sum_{i'=1}^{d'} \xi_{i'}\right) \right), \end{aligned} \quad (16)$$

where $\psi_0(\cdot)$ is the digamma function. Note that $D_{KL}(q(z|y)||p(z))$ and $D_{KL}(q(z|h, y)||p(z))$ have the same form, since $q(z|y)$ and $q(z|h, y)$ both follow Gaussian distributions parameterized by DNNs, while the difference lies in the parametric forms of μ_i and m_i^2 as can be seen in (9) and (11). The first term in either (13) or (14) can not be analytically calculated due to the intractable integral. Nevertheless, reparameterization trick [21, 38, 9] can be applied to obtaining an unbiased gradient estimator for it, which has been integrated into modern deep learning frameworks like PyTorch [36].

Given a training dataset \mathcal{D} , we now can optimize the network parameters Ψ and Φ with respect to the ELBO (13) or (14), over all data in \mathcal{D} , which respectively corresponds to the following objectives:

$$\max_{\Psi, \Phi} \sum_{j=1}^N \mathcal{L}_{KF}(y^{(j)}; \Psi, \Phi), \quad \max_{\Psi, \Phi} \sum_{j=1}^N \mathcal{L}_{KD}(y^{(j)}; \Psi, \Phi). \quad (17)$$

Remark: The three terms involved in the ELBO, either \mathcal{L}_{KF} or \mathcal{L}_{KD} , play important roles. Firstly, the second term plays the role of supervising *Deblur-Net* by the clean training image, which acts similarly as the loss functions of most end-to-end trained deblurring DNNs. Secondly, the third term provides supervision information to *Kernel-Net*, which is often ignored in many existing methods. Thirdly, the first term (likelihood), attributed to the physical blur model, includes both *Deblur-Net* and *Kernel-Net*, making them interact with each other, which is also less considered in previous methods. To summarize, with the derived ELBO, *Deblur-Net* and *Kernel-Net* can both be supervised by data-driven priors and interact with each other during the training process.

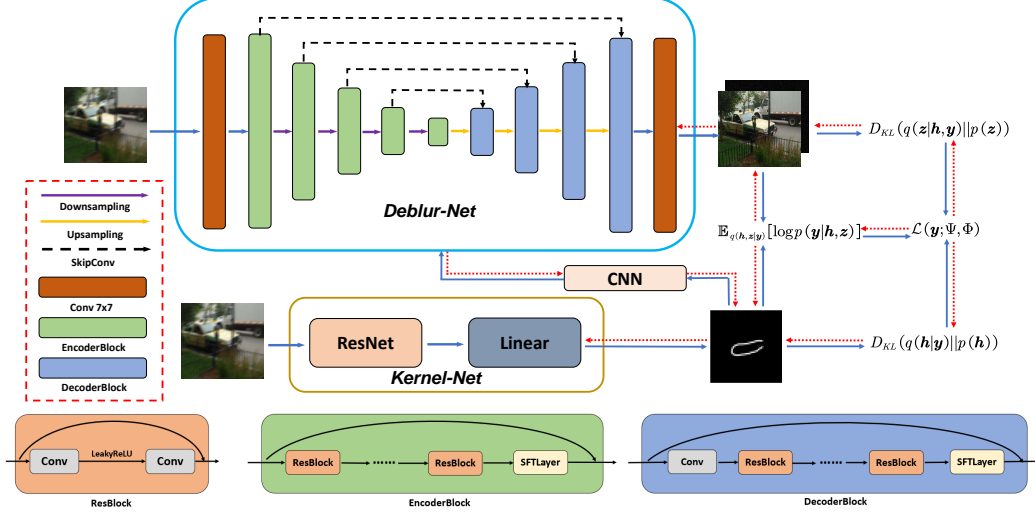


Figure 1: The architecture of the proposed framework with kernel-dependent inference structure.

3.4 Network Architecture

Design of *Deblur-Net*: For the kernel-free inference structure for z , we design a relative simple yet effective baseline *Deblur-Net* for evaluation. We adopt the widely used U-Net [41], with four scales in the encoder and decoder, to capture multi-scale features of an image, and make some modifications to it. Specifically, we first use the modified ResBlock in [30] but replace the ReLU activation with LeakyReLU one and use a small kernel size of 3. Then we stack a series of ResBlocks (the number of ResBlocks varies in our experiments depending on different purposes) to construct the encoding and decoding blocks. The number of channels at all layers is set to 64. The downsample is done by a convolution layer with filter size 3 and stride 2, while the upsample by a transposed convolution layer with filter size 5 and stride 2.

For the kernel-dependent inference structure for z , the *Deblur-Net* should also take the blur kernel, in addition to the blurry image, as its input. To do so, we adopt the SFT layer in [13] to the encoding and decoding blocks. We also use a sub-network to map the blur kernel from matrix to vector.

Design of *Kernel-Net*: We use a ResNet [16] as feature extractor for *Kernel-Net*, followed by a linear transformation layer. Then we apply a softmax layer after that and rescale it to make the final output non-negative and normalized. It should be mentioned that accurately estimating the blur kernel is not a easy task, and there is still a large room to improve the this baseline *Kernel-Net*.

The overall network architecture of the proposed framework with kernel-dependent inference is illustrated in Fig. 1. For the kernel-free inference, the architecture is almost the same, except that the output of *Kernel-Net* does not be input to *Deblur-Net*.

3.5 Further Discussions

Non-uniform Blur: Our deblurring framework is constructed based on the physical blur model (1), which assumes uniform blur kernel across the spatial domain. For non-uniform blurring, we can follow previous studies [33, 32], and treat the blur kernel locally uniform within a relatively small image patch. Since in the training phase, we indeed train the inference networks with patches cropped from images in the training set, the local uniformity of the blur kernel approximately holds, and therefore the proposed framework is also applicable. In the testing phase, the kernel-free inference can be done without any specific modification, while the kernel-dependent inference can be implemented by first performing deblurring on overlapping image patches and then aggregating them to obtain the final result, just like many traditional image restoration methods [7, 14]. However, the above strategy is only a rough approximation, and the application to non-uniform deblurring is still a major limitation of the proposed framework, which should be further investigated in future.

Relationship to Kernel-involved Methodologies: In previous studies, there are mainly two different methodologies in deep learning based deblurring methods that take the kernel information into consideration. The first is represented by Pan *et al.*[32], who introduced a loss term motivated by the

physical blur model (1). This loss term plays the similar role as the likelihood in ELBOs (13) and (14) under our framework. The second is by Kaufman *et al.*[19], who designed a network to estimate the blur kernel from the blurry image, and input the estimated kernel to the main deblurring network as auxiliary information. This strategy is consistent with the kernel-dependent inference structure for z under our framework. Compared with the two existing kernel-involved methodologies, our framework provides a more complete and concise unification, naturally by Bayesian inference principle without any tricky designing, which can not only explain the effectiveness of the existing method from Bayesian perspective, but also facilitate to network training as demonstrated in experiments.

Incorporating with Existing Networks: Though we have designed simple baseline networks in Section 3.4, our proposed framework is indeed very general, and can be incorporated with any existing DNNs designed for image deblurring task, as training guidance. As verified in Section 4.4, the performance can be improved by virtue of the our Bayesian modeling and learning framework.

4 Experimental Results

In this section, we present the experimental results of the proposed blind image deblurring framework, in comparison with current state-of-the-art methods. We call our method *Variational Bayesian Deblurring Network*, denoted as VBDeblurNet. More results are provided in Appendix C.

4.1 Experiment Settings

Datasets: We evaluate the proposed method mainly on three datasets that are widely used for evaluating the deep learning based image deblurring methods, including *Text* by Hradíš *et al.*[17], *RealBlur* by Rim *et al.*[40] and *GoPro* by Nah *et al.*[30]. The three datasets represent typical situations we may encounter when applying a deep learning based method. Specifically, the *Text* dataset is composed of blurry-clean-kernel image tuples with uniform blur, 60,000 for training and 1,000 for testing; the *RealBlur*² dataset contains 3,758 blurry-clean image pairs for training and 980 for testing, while the blur kernels are approximately uniform; and the *GoPro* dataset consists of 2,103 blurry-clean training pairs from 22 sequences and 1,111 testing pairs from 11 sequences, with non-uniform blur kernels. As mentioned in Section 3.1, on the latter two datasets, the prior information of kernels can be estimated from training patches.

Implementation: The weights of networks are initialized according to [15]. In each iteration, we randomly crop the entire images to a size of 256×256 patch for training. The Adam optimizer [20] using default parameters is adopted for training, with initial learning rate $1e-4$, and being reduced to $1e-5$ as loss becoming stable and finally to $1e-6$. Without explicitly specified, we set the hyper-parameter σ^2 in (2) to $1e-5$, ε_0^2 in (3) to $1e-6$, and c in (6) to $2e4$, respectively. Analyses for the effects of these hyper-parameters are provided in Appendix B.

4.2 Model Verification and Ablation Study

We first construct experiments to verify the effectiveness of the proposed framework with ablation study. Since the *Text* dataset contains the complete and accurate information of blur kernels, we can use it to fully verify the effectiveness of the proposed framework. For a illustration purpose, we use a relatively small *Deblur-Net* with 4 ResBlocks in each encoding or decoding block of the U-Net. We consider four strategies, with different loss functions and inference structures, for obtaining a deblurring network. The first two are training under the supervision of naive mean squared error (MSE), with kernel-free and kernel-dependent inference structures, which are respectively denoted as MSE_{KF} and MSE_{KD} . The latter two are the proposed framework with kernel-free and kernel-dependent inference structures, denoted as $VBDeblurNet_{KF}$ and $VBDeblurNet_{KD}$, respectively.

The deblurring performance of each strategy, in terms of *peak signal-to-noise-ratio* (PSNR) and *structure similarity* (SSIM) [48], is summarized in Table 1. As can be seen from the table, with the same inference structure, the performance can be largely improved by virtue of the proposed VBDeblurNet framework. Besides, even with the simpler kernel-free inference structure, the proposed $VBDeblurNet_{KF}$ can outperform MSE_{KD} that uses kernel information in inference. These results evidently verify the effectiveness of the proposed framework.

²We use the *RealBlur-J* subset in experiments.

Table 1: Deblurring results on *Text* dataset, with different loss functions and inference structures. The best and the second best results are highlighted in bold and Italic bold, respectively.

Method	MSE _{KF}	VBDeblurNet _{KF}	MSE _{KD}	VBDeblurNet _{KD}
PSNR	28.70	29.07	29.06	29.58
SSIM	0.9845	0.9860	0.9846	0.9855

Table 2: Comparison of competing methods in terms of PSNR and SSIM on *Text* dataset.

Method	Xu <i>et al.</i> [49]	Pan <i>et al.</i> [35]	Hradiš <i>et al.</i> [17]	Nah <i>et al.</i> [30]	Pan <i>et al.</i> [32]	Kaufman <i>et al.</i> [19]	VBDeblurNet _{KF}	VBDeblurNet _{KD}
PSNR	17.52	18.47	26.53	26.81	28.80	27.90	29.70	30.38
SSIM	0.4186	0.6127	0.9422	0.9743	0.9744	0.9604	0.9862	0.9872

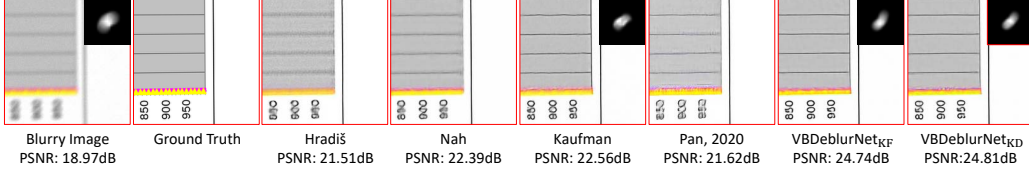


Figure 2: Visual deblurring results of competing methods on *Text* dataset, together with the estimated blur kernels if available.

Table 3: Comparison of competing methods in terms of PSNR and SSIM on *RealBlur-J* dataset.

Method	Hu <i>et al.</i> [18]	Xu <i>et al.</i> [49]	Pan <i>et al.</i> [35]	DeblurGAN-v2 [25]	SRN [46]	MPRNet [51]	VBDeblurNet _{KF}	VBDeblurNet _{KD}
PSNR	26.41	27.14	27.22	29.69	31.38	31.76	31.85	31.73
SSIM	0.8028	0.8303	0.7901	0.8703	0.9091	0.9220	0.9132	0.9106

4.3 Comparison with State-of-the-art Methods

In this subsection, we compared the proposed method with state-of-the-art methods, including traditional optimization-based methods [49, 34, 35, 18] and deep learning-based methods [17, 30, 32, 37, 24, 25, 51, 53, 52], on the three datasets introduced in Section 4.1. The *Deblur-Net* used here is with 6 Resblocks in each encoding or decoding block, in order to achieve a good performance. We show the quantitative results in terms of two commonly used metrics, PSNR and SSIM, in Tables 2, 3 and 4. Note that the competing methods on different datasets are also different. This is because that we want to make sure that each deep learning based method has been trained and tested on the same dataset, by either citing the results from corresponding papers or retraining the models by ourselves.

It can be seen from Tables 2 that, both versions of the proposed framework significantly improve the previous state-of-the-art results on *Text* dataset. This is not surprising, since the structure of the training image tuples in this dataset can be faithfully characterized by our proposed Bayesian generative model, and thus the performance can be naturally benefited by our deep variational inference framework. On the other two datasets, although the groundtruth blur kernels are unavailable, the benefits of the proposed framework can also be clearly observed from Tables 3 and 4. Specifically, the proposed method performs at least comparable with the current state-of-the-art one, i.e., MPRNet, in terms of both PSNR and SSIM, especially that it outperforms MPRNet on *RealBlur-J* dataset in terms of PSNR. The promising performance of MPRNet is not surprising, since authors have made a lot of efforts in network designing. Comparatively, our DNN architecture is much simpler, mainly built on classic structures, such as U-Net and ResBlock, and its performance is mostly attributed to the proposed VBDeblurNet framework. From this perspective, these quantitative results indeed substantiate the effectiveness of the proposed framework. Besides, we can also straightforwardly apply our framework to MPRNet, in order to further pursue better performance.

For a more intuitive illustration, we draw the example visual results in Figs. 2, 3 and 4 on the three datasets, and more results are provided in Appendix C. Fig. 2 shows visual deblurring results an image in *Text* dataset by different deep learning methods contained in Table 2. As can be seen, the deblurred images by our method have better visual quality, especially for producing sharper edges and digits. Compared the two inference structures of our method, kernel-dependent one unsurprisingly performs better in more accurately recovering digit “5”, since it makes full use of the kernel information. Besides, the estimated kernels by our method are also close to the ground truth. For the deblurring example on *RealBlur-J* dataset, shown in Fig. 3, our method produces slightly better results than that of MPRNet both in terms of PSNR and visual quality. Visual results on *GoPro* dataset shown in Fig. 4 are also very interesting. Specifically, although MPRNet achieves higher PSNR, its visual quality is obviously not the best, especially that it fails to recover the number plate on the car. As a comparison,

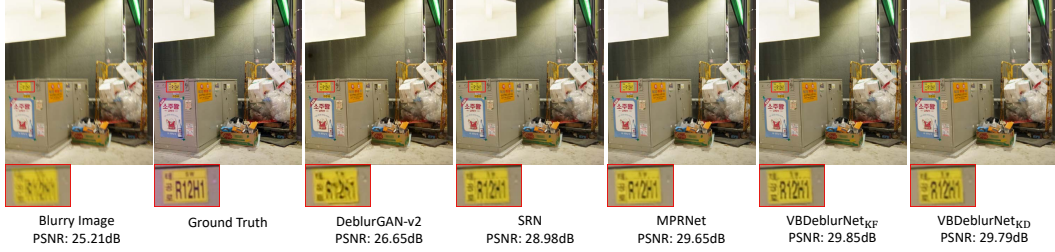


Figure 3: Visual deblurring results of competing methods on *RealBlur-J* dataset.

Table 4: Comparison of competing methods in terms of PSNR and SSIM on *GoPro* dataset.

Method	Nah <i>et al.</i> [30]	DeblurGAN [24]	SRN [46]	Gao <i>et al.</i> [10]	DBGAN [55]	Zhang <i>et al.</i> [52]	MPRNet [51]	VBDeblurNet _{KF}	VBDeblurNet _{KD}
PSNR	29.08	28.70	30.21	30.92	31.10	31.20	32.66	31.87	32.03
SSIM	0.9135	0.858	0.9352	0.9421	0.9424	0.940	0.9589	0.9519	0.9531



Figure 4: Visual deblurring results of competing methods on *GoPro* dataset.

Table 5: Comparison of existing networks trained with MSE and VBDeblurNet on *Text* dataset.

Method	Nah <i>et al.</i> [30]			Kaufman <i>et al.</i> [19]		
	MSE	VBDeblurNet	$\Delta \uparrow$	MSE	VBDeblurNet	$\Delta \uparrow$
PSNR	26.81	27.03	0.22	27.90	28.10	0.20
SSIM	0.9743	0.9756	0.0013	0.9607	0.9636	0.0029

our VBDeblurNet_{KD} method can relatively better recover this number plate, especially for digit “4” within it.

4.4 Enhancing Existing Networks by Proposed Framework

As discussed in Section 3.5, the proposed framework can be incorporated with existing DNNs, to improve their deblurring performances. To verify this, we train on the *Text* dataset two existing deblurring networks, i.e., the ones proposed by Nah *et al.*[30], and Kaufman and Fattal [19], under MSE loss and with our framework, respectively. The former network uses kernel-free inference structure and the latter adopt the kernel-dependent one. The results in terms of PSNR and SSIM are summarized in Table 5. As can be seen from the Table that, the performance of existing networks can be evidently improved by the proposed framework, no matter which types of inference structures they are built on. These improvements can be attributed to two advantages led to by our Bayesian modeling and learning framework. Firstly, the kernel information is naturally included in the training objective as auxiliary supervision. More importantly, *Deblur-Net* and *Kernel-Net* can interact with each other, under the guidance of the likelihood term led to by the physical blur model, to promote the overall training.

5 Conclusion

We have proposed a new deep variational Bayesian framework, i.e., VBDeblurNet, for blind image deblurring, under which, the approximate posterior of the latent clean image and blur kernel, parameterized by DNNs, can be jointly learned in an amortized inference fashion. By virtue of the fully Bayesian formulation, the inference networks for clean image and blur kernel can both be supervised by data-driven priors, and interact with each other by the likelihood attributed to the physical blur model during training, which thus leads to promising deblurring performance. Comprehensive experiments have verified the effectiveness of the proposed framework, showing that it can not only achieve a promising results with relatively simple networks, but also be able to enhance the deblurring performance of existing DNNs. In the future, we will devote to improving the applicability of VBDeblurNet in non-uniform deblurring.

References

- [1] Martin Arjovsky, Soumith Chintala, and Léon Bottou. Wasserstein generative adversarial networks. In *Proceedings of the 34th International Conference on Machine Learning*, volume 70, pages 214–223. PMLR, 2017.
- [2] Tom E Bishop, S Derin Babacan, Bruno Amizic, Aggelos K Katsaggelos, Tony Chan, and Rafael Molina. Blind image deconvolution: problem formulation and existing approaches. In *Blind Image Deconvolution*, pages 21–62. CRC press, 2017.
- [3] Jianrui Cai, Wangmeng Zuo, and Lei Zhang. Dark and bright channel prior embedded network for dynamic scene deblurring. *IEEE Transactions on Image Processing*, 29:6885–6897, 2020.
- [4] Ayan Chakrabarti. A neural approach to blind motion deblurring. In *European conference on computer vision*, pages 221–235. Springer, 2016.
- [5] Tony F Chan and Chiu-Kwong Wong. Total variation blind deconvolution. *IEEE transactions on Image Processing*, 7(3):370–375, 1998.
- [6] Chao Dong, Chen Change Loy, Kaiming He, and Xiaoou Tang. Image super-resolution using deep convolutional networks. *IEEE transactions on pattern analysis and machine intelligence*, 38(2):295–307, 2015.
- [7] Michael Elad and Michal Aharon. Image denoising via sparse and redundant representations over learned dictionaries. *IEEE Transactions on Image Processing*, 15(12):3736–3745, 2006.
- [8] Rob Fergus, Barun Singh, Aaron Hertzmann, Sam T Roweis, and William T Freeman. Removing camera shake from a single photograph. In *ACM SIGGRAPH*, pages 787–794, 2006.
- [9] Mikhail Figurnov, Shakir Mohamed, and Andriy Mnih. Implicit reparameterization gradients. In S. Bengio, H. Wallach, H. Larochelle, K. Grauman, N. Cesa-Bianchi, and R. Garnett, editors, *Advances in Neural Information Processing Systems*, volume 31. Curran Associates, Inc., 2018.
- [10] Hongyun Gao, Xin Tao, Xiaoyong Shen, and Jiaya Jia. Dynamic scene deblurring with parameter selective sharing and nested skip connections. In *Proceedings of the IEEE/CVF Conference on Computer Vision and Pattern Recognition*, pages 3848–3856, 2019.
- [11] Dong Gong, Jie Yang, Lingqiao Liu, Yanning Zhang, Ian Reid, Chunhua Shen, Anton Van Den Hengel, and Qinfeng Shi. From motion blur to motion flow: A deep learning solution for removing heterogeneous motion blur. In *Proceedings of the IEEE conference on computer vision and pattern recognition*, pages 2319–2328, 2017.
- [12] Ian Goodfellow, Jean Pouget-Abadie, Mehdi Mirza, Bing Xu, David Warde-Farley, Sherjil Ozair, Aaron Courville, and Yoshua Bengio. Generative adversarial nets. In *Advances in Neural Information Processing Systems*, volume 27, 2014.
- [13] Jinjin Gu, Hannan Lu, Wangmeng Zuo, and Chao Dong. Blind super-resolution with iterative kernel correction. In *Proceedings of the IEEE/CVF Conference on Computer Vision and Pattern Recognition*, pages 1604–1613, 2019.
- [14] Shuhang Gu, Qi Xie, Deyu Meng, Wangmeng Zuo, Xiangchu Feng, and Lei Zhang. Weighted nuclear norm minimization and its applications to low level vision. *International Journal of Computer Vision*, 121:183–208, 2017.
- [15] Kaiming He, Xiangyu Zhang, Shaoqing Ren, and Jian Sun. Delving deep into rectifiers: Surpassing human-level performance on imagenet classification. In *Proceedings of the IEEE international conference on computer vision*, pages 1026–1034, 2015.
- [16] Kaiming He, Xiangyu Zhang, Shaoqing Ren, and Jian Sun. Deep residual learning for image recognition. In *Proceedings of the IEEE conference on computer vision and pattern recognition*, pages 770–778, 2016.
- [17] Michal Hradiš, Jan Kotera, Pavel Zemčík, and Filip Šroubek. Convolutional neural networks for direct text deblurring. In *Proceedings of BMVC*, volume 10, 2015.
- [18] Zhe Hu, Sunghyun Cho, Jue Wang, and Ming-Hsuan Yang. Deblurring low-light images with light streaks. In *Proceedings of the IEEE Conference on Computer Vision and Pattern Recognition*, pages 3382–3389, 2014.
- [19] Adam Kaufman and Raanan Fattal. Deblurring using analysis-synthesis networks pair. In *Proceedings of the IEEE/CVF Conference on Computer Vision and Pattern Recognition*, pages 5811–5820, 2020.

- [20] Diederik P Kingma and Jimmy Ba. Adam: A method for stochastic optimization. In *Proceedings of the 3rd International Conference on Learning Representations (ICLR)*, 2014.
- [21] Diederik P Kingma and Max Welling. Auto-encoding variational bayes. In *Proceedings of the 2nd International Conference on Learning Representations (ICLR)*, 2014.
- [22] Dilip Krishnan and Rob Fergus. Fast image deconvolution using hyper-laplacian priors. In *Advances in neural information processing systems*, volume 22, pages 1033–1041, 2009.
- [23] Dilip Krishnan, Terence Tay, and Rob Fergus. Blind deconvolution using a normalized sparsity measure. In *Proceedings of the IEEE Conference on Computer Vision and Pattern Recognition*, pages 233–240. IEEE, 2011.
- [24] Orest Kupyn, Volodymyr Budzan, Mykola Mykhailych, Dmytro Mishkin, and Jiří Matas. Deblurgan: Blind motion deblurring using conditional adversarial networks. In *Proceedings of the IEEE conference on computer vision and pattern recognition*, pages 8183–8192, 2018.
- [25] Orest Kupyn, Tetiana Martyniuk, Junru Wu, and Zhangyang Wang. Deblurgan-v2: Deblurring (orders-of-magnitude) faster and better. In *The IEEE International Conference on Computer Vision (ICCV)*, Oct 2019.
- [26] Anat Levin, Yair Weiss, Fredo Durand, and William T Freeman. Understanding and evaluating blind deconvolution algorithms. In *2009 IEEE Conference on Computer Vision and Pattern Recognition*, pages 1964–1971. IEEE, 2009.
- [27] Tomer Michaeli and Michal Irani. Blind deblurring using internal patch recurrence. In *European conference on computer vision*, pages 783–798. Springer, 2014.
- [28] Rafael Molina, Aggelos K Katsaggelos, Javier Abad, and Javier Mateos. A bayesian approach to blind deconvolution based on dirichlet distributions. In *1997 IEEE international conference on acoustics, speech, and signal processing*, volume 4, pages 2809–2812. IEEE, 1997.
- [29] Rafael Molina, Javier Mateos, and Aggelos K Katsaggelos. Blind deconvolution using a variational approach to parameter, image, and blur estimation. *IEEE Transactions on Image Processing*, 15(12):3715–3727, 2006.
- [30] Seungjun Nah, Tae Hyun Kim, and Kyoung Mu Lee. Deep multi-scale convolutional neural network for dynamic scene deblurring. In *Proceedings of the IEEE conference on computer vision and pattern recognition*, pages 3883–3891, 2017.
- [31] Sungchan Oh and Gyeonghwan Kim. Robust estimation of motion blur kernel using a piecewise-linear model. *IEEE transactions on image processing*, 23(3):1394–1407, 2014.
- [32] Jinshan Pan, Jiangxin Dong, Yang Liu, Jiawei Zhang, Jimmy Ren, Jinhui Tang, Yu Wing Tai, and Ming-Hsuan Yang. Physics-based generative adversarial models for image restoration and beyond. *IEEE transactions on pattern analysis and machine intelligence*, 2020.
- [33] Jinshan Pan, Zhe Hu, Zhixun Su, Hsin-Ying Lee, and Ming-Hsuan Yang. Soft-segmentation guided object motion deblurring. In *Proceedings of the IEEE Conference on Computer Vision and Pattern Recognition*, pages 459–468, 2016.
- [34] Jinshan Pan, Zhe Hu, Zhixun Su, and Ming-Hsuan Yang. Deblurring text images via l0-regularized intensity and gradient prior. In *Proceedings of the IEEE Conference on Computer Vision and Pattern Recognition*, pages 2901–2908, 2014.
- [35] Jinshan Pan, Deqing Sun, Hanspeter Pfister, and Ming-Hsuan Yang. Blind image deblurring using dark channel prior. In *Proceedings of the IEEE Conference on Computer Vision and Pattern Recognition*, pages 1628–1636, 2016.
- [36] Adam Paszke, Sam Gross, Francisco Massa, Adam Lerer, James Bradbury, Gregory Chanan, Trevor Killeen, Zeming Lin, Natalia Gimelshein, Luca Antiga, Alban Desmaison, Andreas Kopf, Edward Yang, Zachary DeVito, Martin Raison, Alykhan Tejani, Sasank Chilamkurthy, Benoit Steiner, Lu Fang, Junjie Bai, and Soumith Chintala. Pytorch: An imperative style, high-performance deep learning library. In H. Wallach, H. Larochelle, A. Beygelzimer, F. d'Alché-Buc, E. Fox, and R. Garnett, editors, *Advances in Neural Information Processing Systems*, volume 32. Curran Associates, Inc., 2019.
- [37] Dongwei Ren, Kai Zhang, Qilong Wang, Qinghua Hu, and Wangmeng Zuo. Neural blind deconvolution using deep priors. In *Proceedings of the IEEE/CVF Conference on Computer Vision and Pattern Recognition*, pages 3341–3350, 2020.

- [38] Danilo Jimenez Rezende, Shakir Mohamed, and Daan Wierstra. Stochastic backpropagation and approximate inference in deep generative models. In *International conference on machine learning*, pages 1278–1286. PMLR, 2014.
- [39] William Hadley Richardson. Bayesian-based iterative method of image restoration. *JoSA*, 62(1):55–59, 1972.
- [40] Jaesung Rim, Haeyun Lee, Jucheol Won, and Sunghyun Cho. Real-world blur dataset for learning and benchmarking deblurring algorithms. In *European Conference on Computer Vision*, pages 184–201. Springer, 2020.
- [41] Olaf Ronneberger, Philipp Fischer, and Thomas Brox. U-net: Convolutional networks for biomedical image segmentation. In *International Conference on Medical image computing and computer-assisted intervention*, pages 234–241. Springer, 2015.
- [42] Christian J Schuler, Michael Hirsch, Stefan Harmeling, and Bernhard Schölkopf. Learning to deblur. *IEEE transactions on pattern analysis and machine intelligence*, 38(7):1439–1451, 2015.
- [43] Qi Shan, Jiaya Jia, and Aseem Agarwala. High-quality motion deblurring from a single image. *ACM Trans. Graph.*, 27(3):1–10, 2008.
- [44] Xingjian Shi, Zhourong Chen, Hao Wang, Dit Yan Yeung, Wai Kin Wong, and Wang Chun Woo. Convolutional lstm network: A machine learning approach for precipitation nowcasting. In *Advances in neural information processing systems*, volume 2015, pages 802–810, 2015.
- [45] Jian Sun, Wenfei Cao, Zongben Xu, and Jean Ponce. Learning a convolutional neural network for non-uniform motion blur removal. In *Proceedings of the IEEE Conference on Computer Vision and Pattern Recognition*, pages 769–777, 2015.
- [46] Xin Tao, Hongyun Gao, Xiaoyong Shen, Jue Wang, and Jiaya Jia. Scale-recurrent network for deep image deblurring. In *Proceedings of the IEEE Conference on Computer Vision and Pattern Recognition*, pages 8174–8182, 2018.
- [47] Dmitry Ulyanov, Andrea Vedaldi, and Victor Lempitsky. Deep image prior. In *Proceedings of the IEEE conference on computer vision and pattern recognition*, pages 9446–9454, 2018.
- [48] Zhou Wang, A.C. Bovik, H.R. Sheikh, and E.P. Simoncelli. Image quality assessment: from error visibility to structural similarity. *IEEE Transactions on Image Processing*, 13(4):600–612, 2004.
- [49] Li Xu, Shicheng Zheng, and Jiaya Jia. Unnatural l0 sparse representation for natural image deblurring. In *Proceedings of the IEEE conference on computer vision and pattern recognition*, pages 1107–1114, 2013.
- [50] Zongsheng Yue, Hongwei Yong, Qian Zhao, Deyu Meng, and Lei Zhang. Variational denoising network: Toward blind noise modeling and removal. In *Advances in Neural Information Processing Systems*, volume 32, pages 1688–1699. Curran Associates, Inc., 2019.
- [51] Syed Waqas Zamir, Aditya Arora, Salman Khan, Munawar Hayat, Fahad Shahbaz Khan, Ming-Hsuan Yang, and Ling Shao. Multi-stage progressive image restoration. In *CVPR*, 2021.
- [52] Hongguang Zhang, Yuchao Dai, Hongdong Li, and Piotr Koniusz. Deep stacked hierarchical multi-patch network for image deblurring. In *Proceedings of the IEEE/CVF Conference on Computer Vision and Pattern Recognition*, pages 5978–5986, 2019.
- [53] Jiawei Zhang, Jinshan Pan, Jimmy Ren, Yibing Song, Linchao Bao, Rynson WH Lau, and Ming-Hsuan Yang. Dynamic scene deblurring using spatially variant recurrent neural networks. In *Proceedings of the IEEE Conference on Computer Vision and Pattern Recognition*, pages 2521–2529, 2018.
- [54] Kai Zhang, Wangmeng Zuo, Yunjin Chen, Deyu Meng, and Lei Zhang. Beyond a gaussian denoiser: Residual learning of deep cnn for image denoising. *IEEE transactions on image processing*, 26(7):3142–3155, 2017.
- [55] Kaihao Zhang, Wenhan Luo, Yiran Zhong, Lin Ma, Bjorn Stenger, Wei Liu, and Hongdong Li. Deblurring by realistic blurring. In *Proceedings of the IEEE/CVF Conference on Computer Vision and Pattern Recognition*, pages 2737–2746, 2020.
- [56] Xu Zhou, Javier Mateos, Fugen Zhou, Rafael Molina, and Aggelos K Katsaggelos. Variational dirichlet blur kernel estimation. *IEEE Transactions on Image Processing*, 24(12):5127–5139, 2015.

A Derivation of the Evidence Lower Bounds

In this section, we derive the evidence lower bounds (ELBOs), or more specifically, Eqs. (13) and (14) in the main text. As presented in the paper, we introduced a variational form of the posterior, denoted as $q(\mathbf{z}, \mathbf{h}|\mathbf{y})$, where we omit the subscripts Ψ, Φ , to approximate the intractable true posterior $p(\mathbf{z}, \mathbf{h}|\mathbf{y})$. Then we have the following decomposition of the marginal log-likelihood:

$$\begin{aligned}
\log p(\mathbf{y}) &= \mathbb{E}_{q(\mathbf{h}, \mathbf{z}|\mathbf{y})} [\log p(\mathbf{y})] \\
&= \mathbb{E}_{q(\mathbf{h}, \mathbf{z}|\mathbf{y})} \left[\log \frac{p(\mathbf{h}, \mathbf{z}, \mathbf{y})}{p(\mathbf{h}, \mathbf{z}|\mathbf{y})} \right] \\
&= \mathbb{E}_{q(\mathbf{h}, \mathbf{z}|\mathbf{y})} \left[\log \frac{q(\mathbf{h}, \mathbf{z}|\mathbf{y}) p(\mathbf{h}, \mathbf{z}, \mathbf{y})}{p(\mathbf{h}, \mathbf{z}|\mathbf{y}) q(\mathbf{h}, \mathbf{z}|\mathbf{y})} \right] \\
&= \mathbb{E}_{q(\mathbf{h}, \mathbf{z}|\mathbf{y})} \left[\log \frac{p(\mathbf{h}, \mathbf{z}, \mathbf{y})}{q(\mathbf{h}, \mathbf{z}|\mathbf{y})} \right] + \mathbb{E}_{q(\mathbf{h}, \mathbf{z}|\mathbf{y})} \left[\log \frac{q(\mathbf{h}, \mathbf{z}|\mathbf{y})}{p(\mathbf{h}, \mathbf{z}|\mathbf{y})} \right] \\
&= \mathbb{E}_{q(\mathbf{h}, \mathbf{z}|\mathbf{y})} \left[\log \frac{p(\mathbf{y}|\mathbf{h}, \mathbf{z})p(\mathbf{h})p(\mathbf{z})}{q(\mathbf{h}, \mathbf{z}|\mathbf{y})} \right] + D_{KL}(q(\mathbf{h}, \mathbf{z}|\mathbf{y})||p(\mathbf{h}, \mathbf{z}|\mathbf{y})) \\
&\triangleq \mathcal{L}(\mathbf{y}; \Psi, \Phi) + D_{KL}(q(\mathbf{h}, \mathbf{z}|\mathbf{y})||p(\mathbf{h}, \mathbf{z}|\mathbf{y})).
\end{aligned} \tag{18}$$

The second term in last line of Eq. (18) is the Kullback-Leibler (KL) divergence between the variational posterior $q(\mathbf{z}, \mathbf{h}|\mathbf{y})$ and the true posterior $p(\mathbf{z}, \mathbf{h}|\mathbf{y})$, which is non-negative, while the first term is the ELBO, which we want to maximize.

For the kernel-free inference structure of \mathbf{z} , we use the basic mean-field assumption for $q(\mathbf{z}, \mathbf{h}|\mathbf{y})$ i.e.,

$$q(\mathbf{z}, \mathbf{h}|\mathbf{y}) = q(\mathbf{z}|\mathbf{y})q(\mathbf{h}|\mathbf{y}). \tag{19}$$

Under this assumption, the ELBO becomes:

$$\begin{aligned}
\mathcal{L}_{KF}(\mathbf{y}; \Psi, \Phi) &= \mathbb{E}_{q(\mathbf{h}, \mathbf{z}|\mathbf{y})} \left[\log \frac{p(\mathbf{y}|\mathbf{h}, \mathbf{z})p(\mathbf{h})p(\mathbf{z})}{q(\mathbf{h}, \mathbf{z}|\mathbf{y})} \right] \\
&= \mathbb{E}_{q(\mathbf{z}|\mathbf{y})q(\mathbf{h}|\mathbf{y})} [\log p(\mathbf{y}|\mathbf{h}, \mathbf{z})] - \mathbb{E}_{q(\mathbf{z}|\mathbf{y})q(\mathbf{h}|\mathbf{y})} \left[\log \frac{q(\mathbf{h}|\mathbf{y})q(\mathbf{z}|\mathbf{y})}{p(\mathbf{h})p(\mathbf{z})} \right] \\
&= \mathbb{E}_{q(\mathbf{z}|\mathbf{y})q(\mathbf{h}|\mathbf{y})} [\log p(\mathbf{y}|\mathbf{h}, \mathbf{z})] - D_{KL}(q(\mathbf{z}|\mathbf{y})||p(\mathbf{z})) - D_{KL}(q(\mathbf{h}|\mathbf{y})||p(\mathbf{h})).
\end{aligned} \tag{20}$$

For the kernel-dependent inference structure of \mathbf{z} , we use the variational form of $q(\mathbf{z}, \mathbf{h}|\mathbf{y})$ by conditional probability rule:

$$q(\mathbf{z}, \mathbf{h}|\mathbf{y}) = q(\mathbf{z}|\mathbf{h}, \mathbf{y})q(\mathbf{h}|\mathbf{y}). \tag{21}$$

Under the setting, the ELBO can be derived as:

$$\begin{aligned}
\mathcal{L}_{KD}(\mathbf{y}; \Psi, \Phi) &= \mathbb{E}_{q(\mathbf{h}, \mathbf{z}|\mathbf{y})} \left[\log \frac{p(\mathbf{y}|\mathbf{h}, \mathbf{z})p(\mathbf{h})p(\mathbf{z})}{q(\mathbf{h}, \mathbf{z}|\mathbf{y})} \right] \\
&= \mathbb{E}_{q(\mathbf{z}|\mathbf{y}, \mathbf{h})q(\mathbf{h}|\mathbf{y})} [\log p(\mathbf{y}|\mathbf{h}, \mathbf{z})] - \mathbb{E}_{q(\mathbf{z}|\mathbf{y}, \mathbf{h})q(\mathbf{h}|\mathbf{y})} \left[\log \frac{q(\mathbf{h}|\mathbf{y})q(\mathbf{z}|\mathbf{y}, \mathbf{h})}{p(\mathbf{h})p(\mathbf{z})} \right] \\
&= \mathbb{E}_{q(\mathbf{z}|\mathbf{y}, \mathbf{h})q(\mathbf{h}|\mathbf{y})} [\log p(\mathbf{y}|\mathbf{h}, \mathbf{z})] - \mathbb{E}_{q(\mathbf{z}|\mathbf{y}, \mathbf{h})q(\mathbf{h}|\mathbf{y})} \left[\log \frac{q(\mathbf{z}|\mathbf{y}, \mathbf{h})}{p(\mathbf{z})} \right] \\
&\quad - \mathbb{E}_{q(\mathbf{z}|\mathbf{y}, \mathbf{h})q(\mathbf{h}|\mathbf{y})} \left[\log \frac{q(\mathbf{h}|\mathbf{y})}{p(\mathbf{h})} \right] \\
&= \mathbb{E}_{q(\mathbf{z}|\mathbf{y}, \mathbf{h})q(\mathbf{h}|\mathbf{y})} [\log p(\mathbf{y}|\mathbf{h}, \mathbf{z})] - \mathbb{E}_{q(\mathbf{h}|\mathbf{y})} [D_{KL}(q(\mathbf{z}|\mathbf{h}, \mathbf{y})||p(\mathbf{z}))] \\
&\quad - D_{KL}(q(\mathbf{h}|\mathbf{y})||p(\mathbf{h})).
\end{aligned}$$

B Hyper-parameter Analysis

In the proposed Bayesian models, there are three hyper-parameters to be tuned, i.e., σ^2 in Eq. (2), ε_0^2 in Eq. (3) and c in Eq. (6) of the main text. Here, we conduct experiments on the *Text* dataset to analyze the effects of these the hyper-parameters.

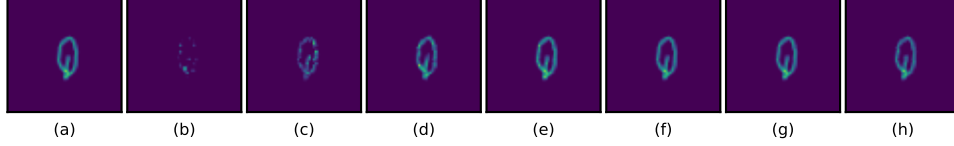


Figure 5: Illustration for the effect of hyper-parameter c . (a): the true blur kernel; (b)-(f): blur kernels sampled with c being set to $1e1$, $1e2$, $1e3$, $5e3$, $1e4$, $2e4$ and $3e4$, respectively.

B.1 The Effect of σ^2

σ^2 measures the noise level of the degenerated images, which should be carefully set. As can be seen in Table 6, the performances are close under when setting σ^2 to $1e-4$ and $1e-5$, and degenerate when setting it too small. This is not surprising, since according to the generation process of the *Text* dataset [17], the standard deviation of the true noise comes from $[0, 7/255]$, which is consistent with the best setting we have found here.

Table 6: Performance under different σ^2 on the *Text* dataset (kernel-free inference structure with 2 ResBlocks in each encoding and decoding block, and fixing ε_0^2 to $1e-4$ and c to $1e4$).

σ^2	1e-4	1e-5	1e-6	1e-7
PSNR	27.51	27.52	27.37	27.03
SSIM	0.9796	0.9796	0.9781	0.9657

B.2 The Effect of ε_0^2

ε_0^2 determines how much does the desired latent clean image z depend on the “clean” training image x . It can be observed from Table 7 that, as ε_0^2 decreasing, the performance first increases and then decreases. This can be naturally explained. Since in the *Text* dataset, the clean training image is indeed the ground truth one, it is better to use a small ε_0^2 . However, if setting ε_0^2 too small, the risk of overfitting increases.

Table 7: Performance under different ε_0^2 on the *Text* dataset (kernel-free inference structure with 2 ResBlocks in each encoding and decoding block, and fixing σ^2 to $1e-6$ and c to $2e4$).

ε_0^2	1e-4	1e-5	1e-6	1e-7
PSNR	26.75	27.00	27.26	27.09
SSIM	0.9638	0.9761	0.9783	0.9779

B.2.1 The Effect of c

c reflects our confidence about the prior information of kernel. Its effect to the kernels sampled from the Dirichlet distribution can be intuitively observed in Fig. 5. Specifically, small c leads to large uncertainty of the sampled kernel, and vice versa. Besides, if c is too small, the sampled kernel will largely deviate from the ground truth one, and therefore relatively larger c is preferred. Also, since in *Text* dataset, the kernels are manually synthesize, we can strongly rely on them, and correspondingly set c to a large value. This is verified by the results in Table 8, that the performance increases as c tends to large. Note that we do not further increase c due to the numerical instability.

Table 8: Performance under different c on the *Text* dataset (kernel-dependent inference structure with 4 ResBlocks in each encoding and decoding block, and fixing σ^2 to $1e-5$ and ε_0^2 to $1e-6$).

c	5e3	1e4	2e4	3e4
PSNR	29.32	29.45	29.48	29.58
SSIM	0.9857	0.9859	0.9859	0.9856

C More Visual Results

In this Section, we provide more visual results on the three datasets we considered in experiments, as shown in Figs. 6, 8 and 7, respectively. These results further substantiate the effectiveness of the proposed method.

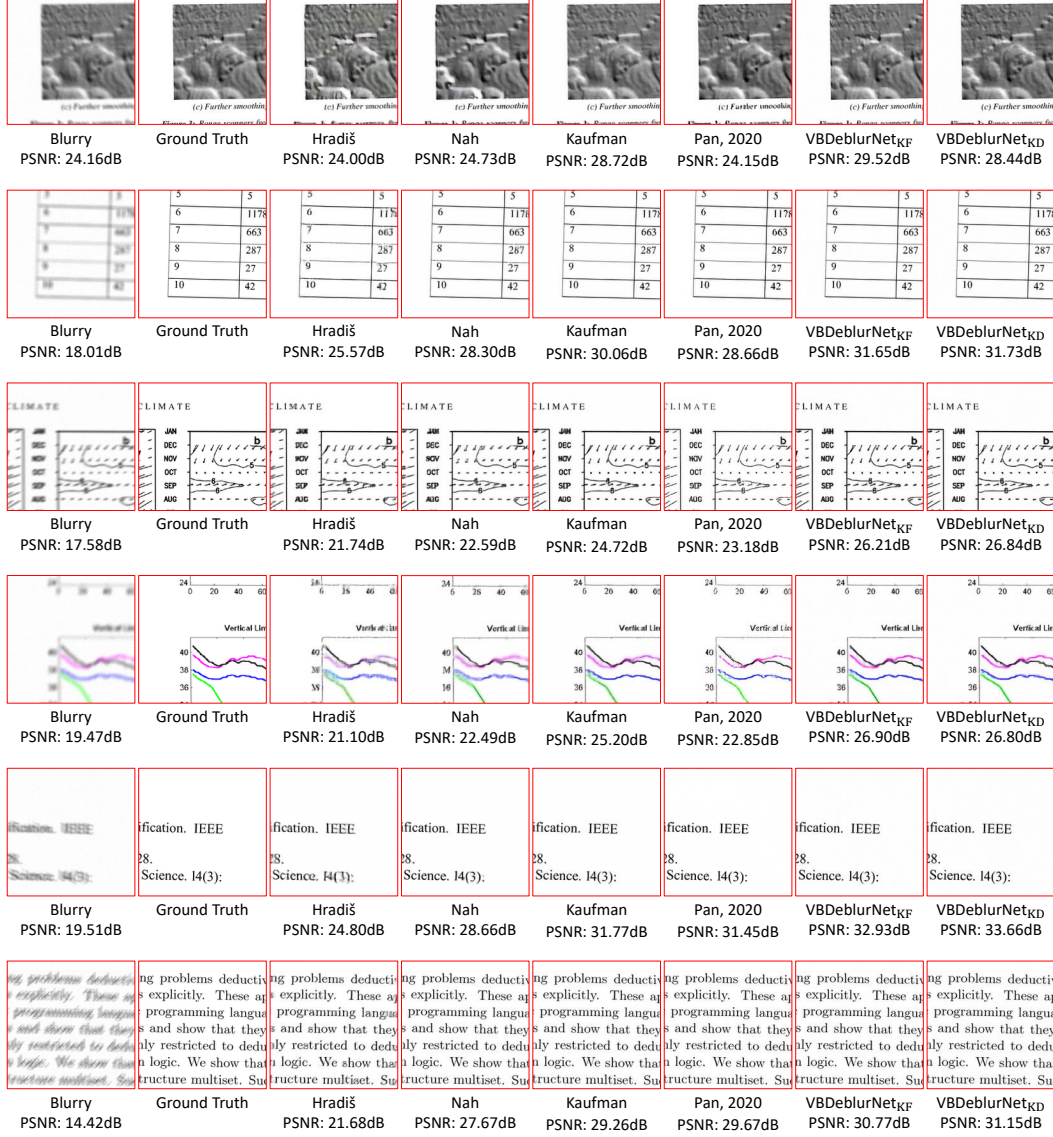


Figure 6: More Visual deblurring results of competing methods on *Text* dataset.

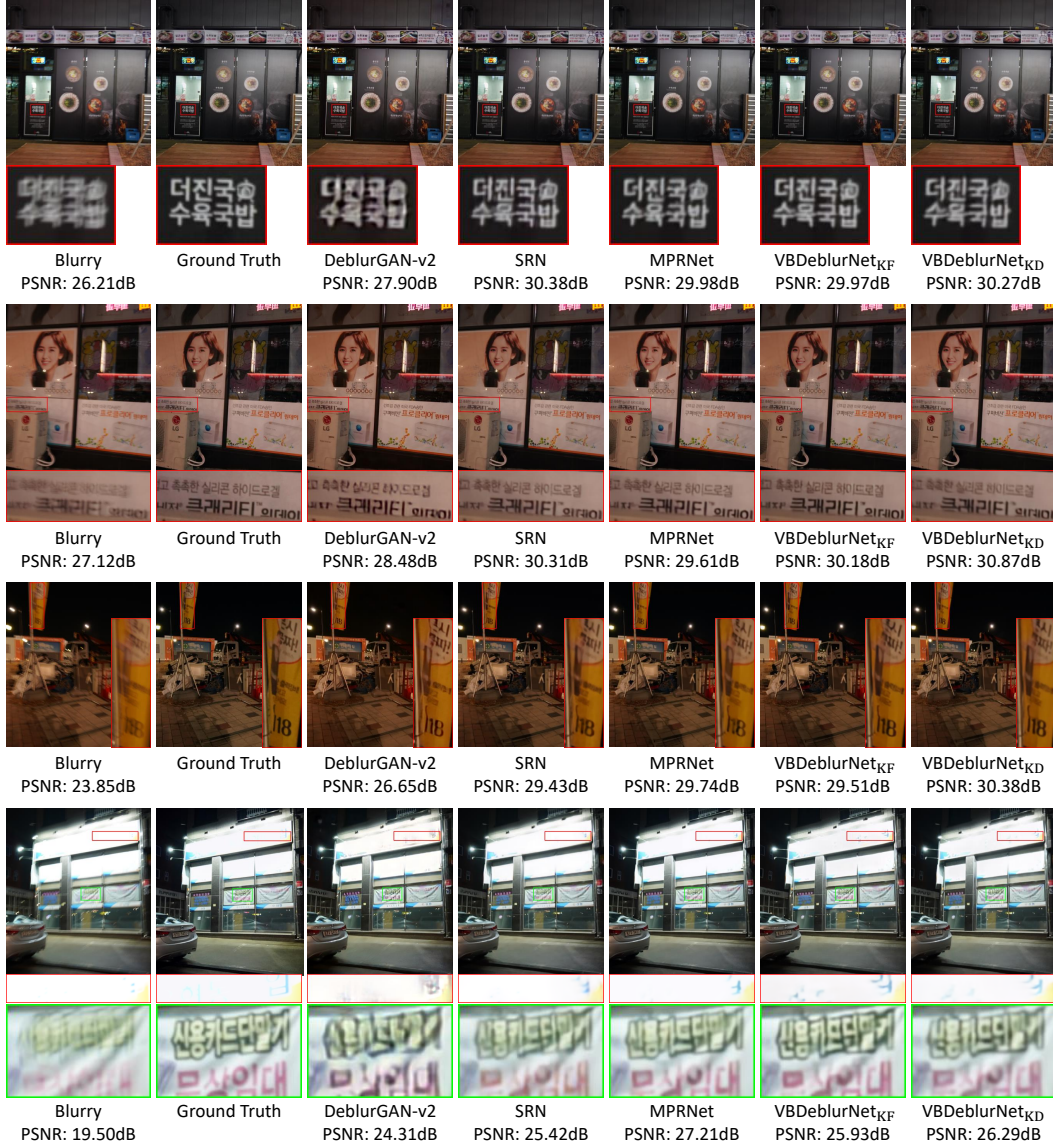


Figure 7: More Visual deblurring results of competing methods on *RealBlur-J* dataset.

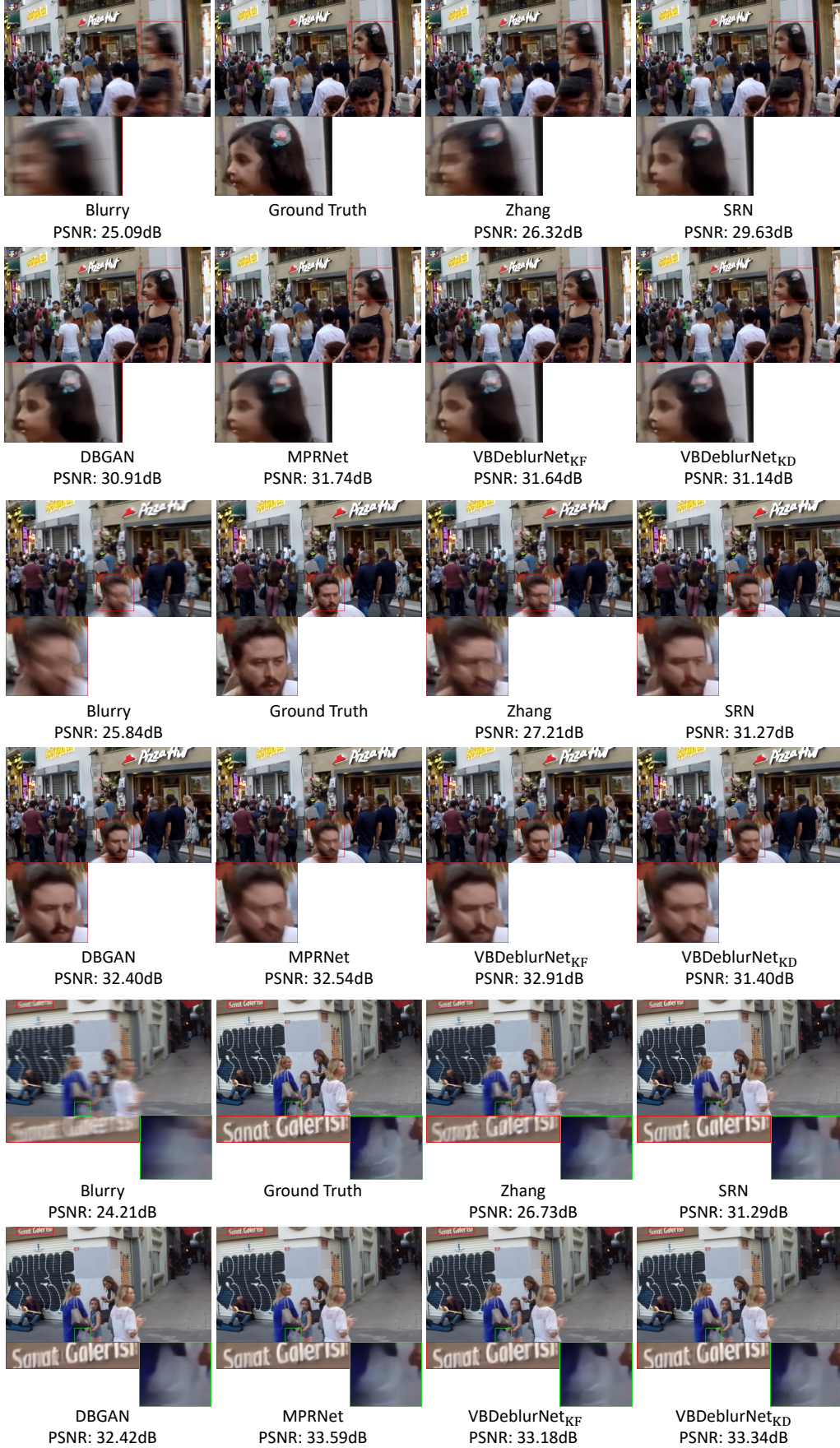


Figure 8: More Visual deblurring results of competing methods on *GoPro* dataset.